

pubs.acs.org/acsaelm Article

A Route towards Fabrication of Functional Ceramic/Polymer Nanocomposite Devices Using the Cold Sintering Process

Sinan Dursun,* Kosuke Tsuji, Sun Hwi Bang, Arnaud Ndayishimiye, and Clive A. Randall

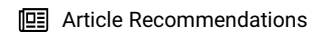


Cite This: ACS Appl. Electron. Mater. 2020, 2, 1917–1924

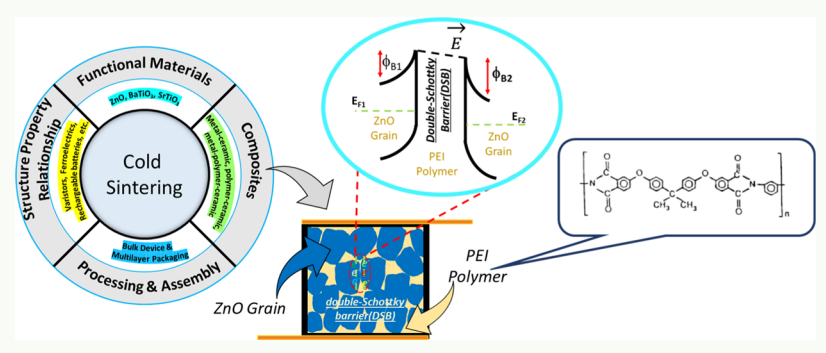


ACCESS I

III Metrics & More



s Supporting Information



ABSTRACT: The use of low-temperature and energy-efficient techniques to fabricate composites with tailored interfaces is currently a topic of growing interest. This study reports the proof of concept of a process to fabricate functional multilayer varistor (MLV) devices below 150 °C. In this MLV device, a small volume fraction of polyetherimide polymer is used to engineer ZnO grain boundaries, and the multilayer composite is cofired with base metal internal electrodes *via* the cold sintering cofired ceramic (CSCC). The resulting dense nanocomposite MLV and controlled nonlinear current—voltage response of the device confirmed the potential of CSCC. This work also opens up the possibility to fabricate multilayer devices for other types of applications.

KEYWORDS: cold sintering, nanocomposite, cofiring, electroceramic multilayer device, varistor

1. INTRODUCTION

The growing technological interest for the miniaturization of low-voltage variable resistor (varistor) devices to integrate in circuit boards has triggered the development of commercial ZnO-based multilayer varistors (MLVs). The functionality is used for the protection of sensitive electronic components from voltage spikes from deleterious electrostatic discharge events, and it is found in systems such as mobile phones, high speed data line, circuit transistors, and so forth. 1-3 MLVs have a wellestablished design to provide lower breakdown voltages and faster response time than metal oxide bulk varistors. These are generally fabricated with low-temperature cofired ceramic technology that allows us to cosinter ceramic layers and internal electrodes in one step, typically in the 700-1000 °C temperature range and with dwell times up to 5 h.4 In conventional cofiring, the different layers of materials need to have the following:

- compatible sintering densification rates to avoid residual stresses creating warpage and cracking.
- controlled and limited chemical interactions to avoid interfacial reactions.
- high relative densities for better mechanical and electrical performances.

Multilayer systems are used in many types of functional devices such as capacitors, inductors, resistors, thermistors, microwave filters, oxygen sensors, actuators, transducers, electronic packages, antennas, thermoelectric generators, solid-state batteries, and solid oxide fuel cells among others. In all these applications, it is also important to have well-controlled dimensionality and excellent performances. $^{5-15}$ The science and engineering of conventional cofiring technologies is well documented. $^{5-9}$

Recently, the cold sintering process (CSP) was unveiled as a technique that enables the sintering of ceramics at low temperatures $(T < 350 \, ^{\circ}\text{C})^{10}$ based on a pressure solution creep mechanism (dissolution \rightarrow mass transport \rightarrow precipitation) induced by the presence of a transient liquid and uniaxial pressure. Several experimental and theoretical studies by ReaxFF molecular dynamics highlighted that the sintering temperature of ZnO with this process can be as low as 120 $^{\circ}\text{C}$,

Received: March 18, 2020 Accepted: June 4, 2020 Published: June 5, 2020





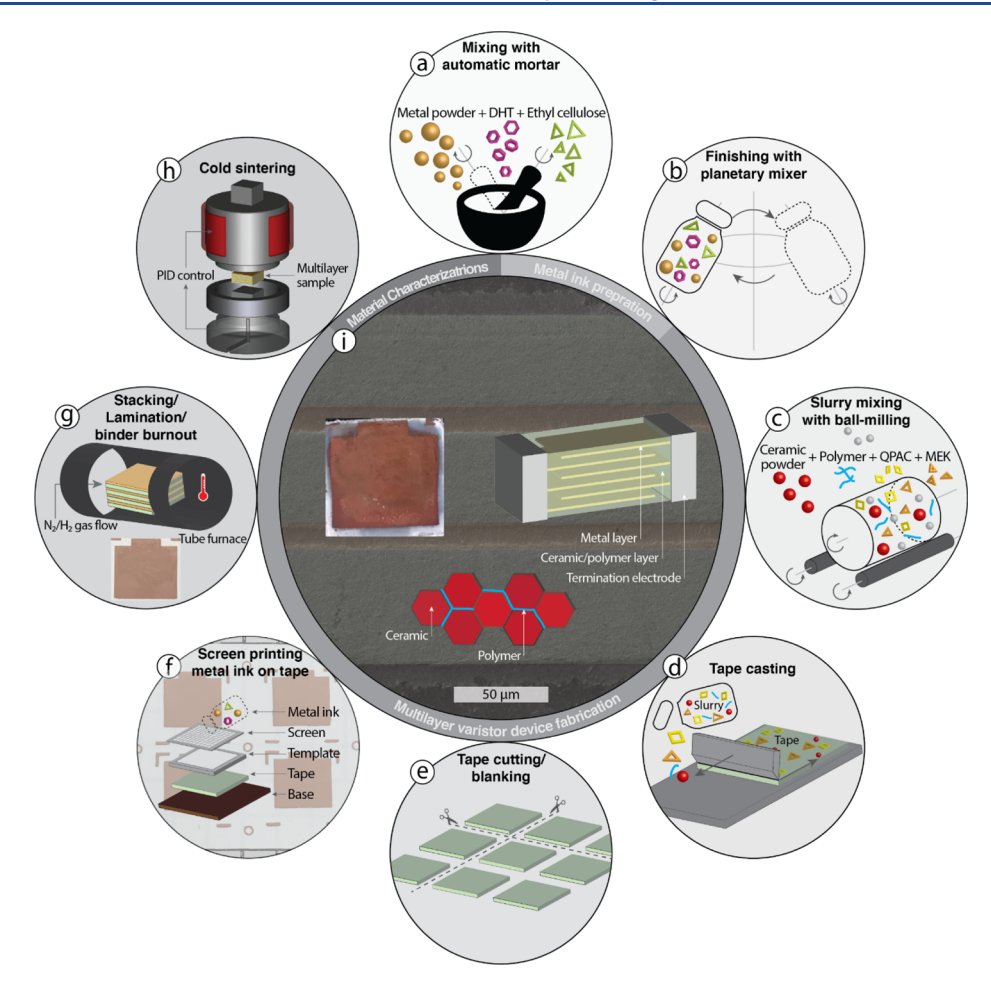


Figure 1. Schematic representation the copper cofired nanocomposite ceramic/polymer MLV device fabricated by CSCC. As shown in the figure, circles correspond: (a,b) metal ink preparation, (c) slurry preparation for tape casting, (d,e) performing of tape casting and cutting, (f) screen printing on the tape, (g) green forming and binder burn out of the multilayer sample under gas flow, (h) CSP, (i) sintered MLV device and the termination of electrodes for the material characterizations.

thanks to solvent-induced accelerated diffusional processes and chemical effects. 12-15 Sintering is typically described as a thermally or mechanically and thermally driven mass transport process to minimize the surface energy of a particle ensemble. For most of the sintering techniques, the ratio between the sintering temperature $(T_{\rm sint})$ and the melting temperature $(T_{\rm melt})$ is in the range of 0.5 < $T_{\rm sint}/T_{\rm melt}$ < 0.95. For cold sintering, this sintering criterion ratio is drastically lower as T_{sint} $T_{\rm melt}$ can be below 0.2. This opens many new opportunities in terms of the low-temperature fabrication of materials, devices, and the integration of all material types, namely, ceramics, polymers, and metals to fabricate all types of composites. As an example, the CSP enabled the fabrication of functional ceramic/ polymer composites with a high-volume fraction of ceramic (up to 99.9%), thanks to the matching of processing temperature windows of ceramic and polymers.¹⁷ The fabrication of dense ceramic/polymer composites, with thermoplastic or thermosetting polymers distributed at the interfaces between adjacent ceramic grains, 18 was demonstrated for multiple applications such as batteries, electronics, and wave propagation among other things: Li₂MoO₄/PTFE (polytetrafluoroethylene),¹⁹ $\text{Li}_{1+x+y}\text{Al}_x\text{Ti}_{2-x}\text{Si}_y\text{P}_{3-y}\text{O}_{12}$ (LATP) with bis-(trifluoromethanesulfonyl)imide (LiTFSI) salts, showing similar room-temperature conductivity (10⁻⁴ S cm⁻¹), comparable to conventionally sintered ceramics 20 (1-x) SiO₂-xPTFE¹⁴

and ZnO–Ca₃Co₄O₉/PTFE.²¹ Recently, Zhao *et al.* presented a new type of nanocomposite structure consisting of ceramic (ZnO) and polymer phases (PTFE—polytetrafluoroethylene) that provide the characteristic varistor I-V behavior.²² Additionally, de Beauvoir *et al.* exhibited applicability of the integration of metallization of different metal types (*i.e.*, Fe, Cu, and Al) into functional electroceramic with the cofiring process as a multilayer form by the enormously low sintering temperature that can be called as the "cold sintering cofired ceramic (CSCC)" process that is reported for the first time in the literature ²³

Furthermore, Bang *et al.*²⁴ recently presented an important step toward manufacturing implementation by lowering the applied pressure by 1 order of magnitude and enabling the size scale-up for functional ceramics manufacturing by cold sintering.

Herein, this paper highlights a route to fabricate functional ZnO-based/polymer nanocomposite MLV devices with copper (Cu) internal electrodes using the CSCC process at temperatures as low as 120 °C (Figure 1). The details of processing steps can be found in the Experimental Section. $I\!-\!V$ measurements and impedance spectroscopy analyses were performed to investigate the structure—property relationship and evaluate the functional properties of the Cu co-fired MLV device.

2. EXPERIMENTAL SECTION

2.1. Fabrication of the Multilayer Device. The fabrication of thick ZnO/PEI (polymer) composite tape was performed by tape casting. The slurry for tape casting was prepared by mixing the appropriate amounts of ZnO powder (Alfa Aesar, Nano powder, 99+% (metals basis), CAS: 1314-13-2) and ULTEM 1000 F3SP PEI powder (SABIC), and a solution composed of the poly(propylene carbonate) (PPC) (QPAC-40, Empower Materials, New Castle, DE) binder was mixed in methyl ethyl ketone (Fisher Chemical) by ball milling for 24 h. $^{34-36}$ The doctor blade gap was adjusted at 150 μ m, and afterward, the tape casting was performed on a Mylar thick film. The tape was held on for an hour for drying, and then, it was cut into squares to a desired size by a laser.

The copper ink was prepared from copper powders that were provided from SHOEI Chemical Inc., Japan. The metal powders were mixed with dihydro terpineol (DHT, Alfa Aesar) and ethyl cellulose in an automatic mortar and pestle, and then, just before the screen printing process, the ink was transferred into a planetary mixer to avoid phase separation because of the settlement of the copper metal. The Cu-metal paste was screen-printed on the composite tapes using the screen. The printed tapes were kept in an oven for drying at 60 °C for 30 min. To assemble the multilayer, two printed tapes were stacked 90° alternatively with five blank composite tapes replaced between them. Five blank composite tapes were put both on the top and bottom as a protective layer, and also, this increases the thickness of the multilayer body for handling the issue right after the multilayer body was pressed lightly at 75 °C to improve the stability of the device. The lamination of the stacked body was carried out (IL4004, Pacific Trinetics Co., San Marcos, CA) at 75 °C under 3000 psi for 30 min. To avoid oxidation of the Cu-inner electrode, binder burn out took place in a mixture of H₂ (5 vol %)/ N_2 (95 vol %) forming gas at 200 °C for 12 h with 0.5 °C heating rate. After debinding, the MLV samples were humidified by 2 M acetic acid solution at 80 °C for 15 min to get a weight gain around 6 wt %. The cold sintering procedure was employed in the stainless steel die and uniaxially pressed at 125 MPa right after the die was heated to the sintering temperature with a 18 °C/min ramp. Two different sintering temperatures were employed in this work, 120 and 220 °C for 30 min. After sintering, the multilayer terminals were polished gently to expose the inner electrode on both sides. Air-dry silver (Pelco Colloidal silver liquid, Ted Pella, Inc., CA) was used for termination to provide electrical contacts from inner Cu-electrodes.

2.2. Characterization. The microstructure and electrical characterization were carried out for the copper cofired nanocomposite ceramic/ polymer MLV device. For microstructure analysis, the samples were placed properly in an epoxy holder, and iridium was sputtered on the polished fractured cross-section of the multilayer. Scanning electron microscopy (SEM) and energy-dispersive X-ray spectroscopy (EDX) were performed with a FEI Nova NanoSEM 630 to evaluate the quality of the multilayer microstructure and investigate interfaces between ceramic, polymer, and metal phases which are, respectively, ZnO, polyetherimide (PEI), and Cu inner electrode in our system. Transmission electron microscopy (TEM) samples were prepared using a FEI Helios 660 focused-ion beam (FIB) system to make the samples electron-transparent for TEM images. A high-resolution transmission electron microscope (FEI Talos, F200X, Eindhoven, Netherlands) was used for high-resolution TEM (HR-TEM) imaging and scanning transmission electron microscopy (STEM) imaging. All the STEM images were captured using a high-angle annular dark field (HAADF) detector. Energy-dispersive X-ray spectroscopic elemental maps of the sample surface were collected using a SuperX EDS scanning system under the STEM mode which has four detectors surrounding the sample. The cold-sintered ZnO/PEI composites (7.5 vol % PEI) at different temperatures as well as the raw PEI polymer were analyzed using a Fourier transformed infrared spectroscopy by attenuated total reflectance (FTIR-ATR), with a Bruker VERTEX 70 FTIR spectrometer (Billerica, MA), equipped with a liquid nitrogen-cooled MCT detector. Spectra were collected at room temperature from an average of 200 scans in the $500-4000 \text{ cm}^{-1}$ range. The I-Vmeasurements were performed with the pA meter (HP4140B, Hewlett

Packard, Palo Alto, CA). The impedance spectroscopy of the multilayer devices was measured with a Modulab XM and Delta oven (Delta 9023, Chou Inc.) under an applied voltage signal of 0.5 V amplitude, in the -75 to +75 °C temperature range.

3. RESULTS AND DISCUSSION

The integration of base metals such as Cu, Fe, Al, and Cu/Fe composite in the fabrication of multilayer systems, sintered at 260 °C by the CSP, were previously demonstrated by de Beauvoir *et al.*²³ Herein, we implemented a similar methodology to fabricate a polymer (PEI) and ceramic-phase (ZnO) nanocomposite MLV with Cu as an inner electrode. To avoid the thermal degradation of the PEI polymer, which has a glass transition temperature of ~225 °C and a decomposition temperature of ~250 °C in air, ²⁵ processing temperatures were decreased to 220 and 120 °C in N_2/H_2 mixture (Figure 1).

Figure 2a shows the infrared spectra of cold-sintered bulk composites at different temperatures as well as the raw PEI

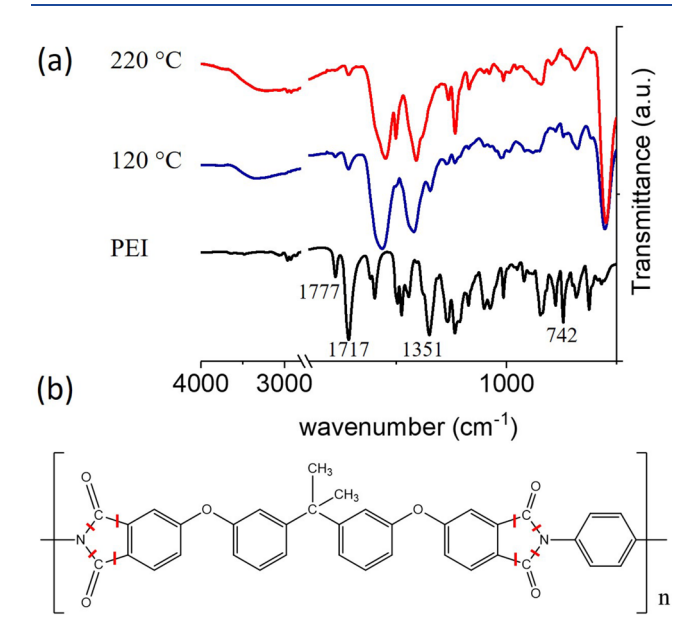


Figure 2. (a) Infrared spectra of PEI and ZnO/PEI composites coldsintered at different temperatures and (b) carboxyl-induced chain breaking mechanism proposed by Farong *et al.*²⁸

polymer. The theoretical density of composites (5.2808 g/cm³) were calculated from the volume fractions and theoretical densities of ZnO and PEI using the mixing law, ²² and the relative density of the bulk ZnO/PEI composites was confirmed >95% using the Archimedes method. The spectra analysis is verified specifically on infrared bands, highlighting intensity changes with the sintering temperature. Infrared bands located at 1720 and 1780 cm⁻¹ are assigned to stretching vibrations of C=O bonding in the imide carbonyl group. 26,27 The 743 and 1355 cm⁻¹ infrared bands are assigned to C-N bending and stretching vibrations.²⁶ For sintering temperatures of 220 °C, we may have a carboxyl-induced PEI chain breaking mechanism (Figure 2b). This degradation mechanism was explained by Farong et al.²⁸ using mass spectroscopy, and here, it is confirmed by the simultaneous and almost total disappearance of infrared bands assigned to imide carbonyl groups ($\overline{1720}$ and 1780 cm⁻¹) and infrared bands of the C-N bonding (743 and 1355 cm⁻ also illustrated in Figure 2b. According to the FTIR results, the sintering temperature of 120 °C would be more appropriate for the fabrication of the ZnO-based/polymer MLV device with Cu inner electrodes, without decomposing the PEI polymer that would limit the insulation performance and results of the device that sintered at 220 °C can be found in the Supporting Information of this paper.

The photograph of a sintered copper cofired ZnO/PEI MLV device is presented in Figure 3a. It is important to emphasize

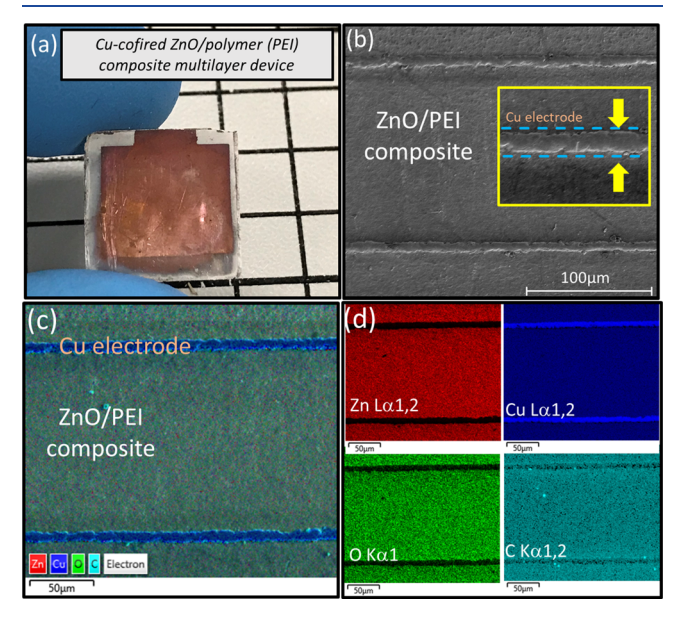


Figure 3. (a) Representative picture of the Cu-co-fired ZnO/polymer (PEI) composite multilayer device sintered at 120 °C for 30 min, (b) SEM image from the multilayer polished cross-section, and (c,d) EDS mapping polished cross-section.

that the well-shaped and defect-free copper electrode at the surface of device is obtained. To investigate the microstructure and elemental distributions of the ceramic/polymer composite and metal layer in the multilayer, SEM and energy dispersive spectroscopy (EDS) were performed on a polished cross-section of the MLV device that is sintered at 120 °C. The copper metal layer and ZnO/PEI composite particulates are effectively cofired and densified after cold sintering (Figure 3b). The inner electrode and composite layers remain parallel with uniform

thicknesses across the samples, without any obvious sign of delamination or intrusion of Cu-metals toward the ceramic/polymer composite phase. Both these observations are further confirmed by EDS mapping (Figure 3c,d).

To present more details in terms of the intergranular nanostructure of the MLV device and the polymer distribution at the interface between ZnO grains, TEM and STEM—EDS were performed. Figure 4 shows TEM and STEM—EDS images of both ceramic/polymer/metal and ceramic/polymer interfaces in the cold-sintered MLV device. Figure 4a represents a multilayer body, and the rectangular frames show different spots of the multilayer device being examined by TEM. STEM—EDS images (Figure 4b,c) confirm that a clean interface of Cu/ZnO/PEI is obtained at a nanoscale and that the interdiffusion between the Cu metal and ZnO/PEI does not occur, as opposed to the device fabricated at 220 °C (Figure S1 in the Supporting Information) where interdiffusion may occur (Figure S2b,c in the Supporting Information).

The TEM image in Figure 4d shows a thickness of the PEI polymer at the interface between two grains ranging between 5 and 10 nm, as desired. The HAADF-STEM and EDS images at lower magnification (Figure 4e,i) shows that PEI is homogeneously distributed at interfaces between ZnO grains. The CSCC enabled the cosintering of the metal, polymer, and ceramic to fabricate functional MLV devices with a new methodology having all process steps below 200 °C, including sintering which takes place at 120 °C only. This would not have been possible with conventional methods as high temperatures required to densify the ceramic would have led to the complete decomposition of the polymer. To the best of our knowledge, this is the lowest sintering temperature that can be found in the literature to fabricate functional ZnO-based MLV devices.

The structure—electrical property relationship of this newtype functional multilayer nanocomposite varistor can be demonstrated by impedance characterization. The impedance spectroscopy is a well-known technique to investigate electrical properties and transport in various materials. It can be utilized to identify conduction mechanisms in the composite and to assess microstructural contributions by fitting data to equivalent circuits.²⁹ The impedance and modulus complex formalisms with real and imaginary contributions are given eqs 1 and 2, respectively

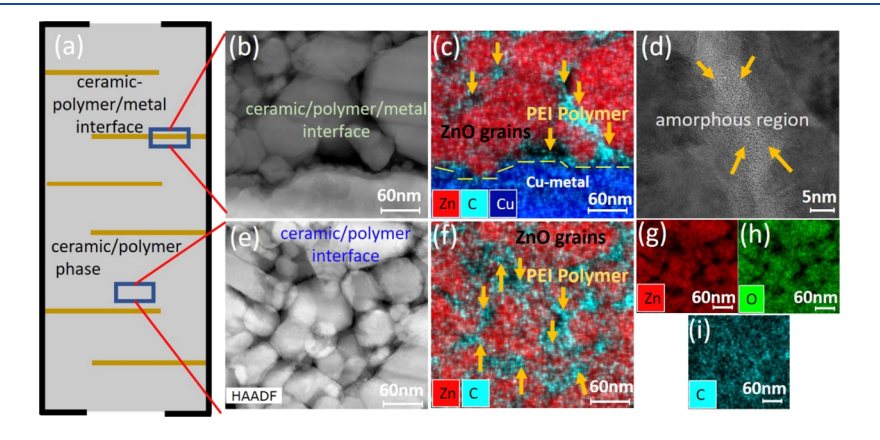


Figure 4. Hierarchical microstructural analysis of copper cofired ceramic/polymer nanocomposite multilayer devices sintered at 120 °C for 30 min. (a) Schematic representation of regions in the multilayer device examined by TEM. (b) HAADF—STEM and (c) elemental mapping by EDS of the interfacial region between the ZnO/PEI composite and Cu-inner layer. (d) HR-TEM of the grain interface between ZnO grains in the ZnO/PEI composite. (e) HAADF—STEM and (f) EDS map of the ZnO/PEI composite zone, with individual elemental mapping of (g) zinc (Zn), (h) oxygen (O), and (i) carbon (C) to highlight the presence of polymers at the interface between ZnO grains.

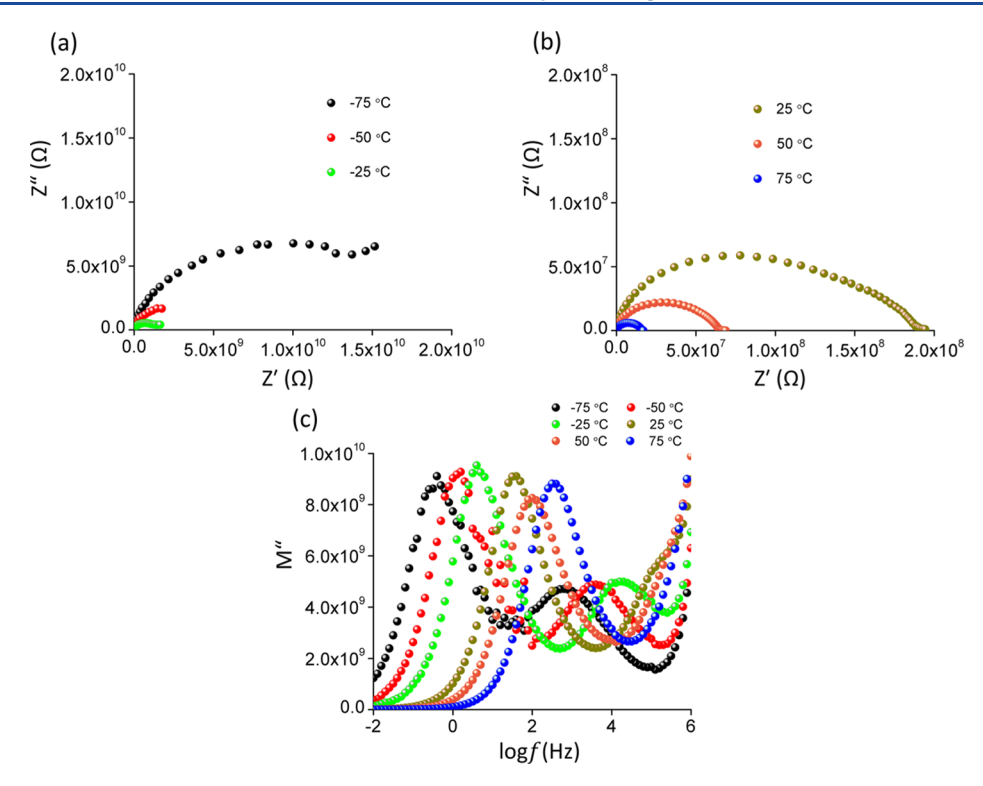


Figure 5. (a,b) Impedance and (c) electrical modulus spectroscopy of cofired composite MLVs cold-sintered at 120 °C as a function of temperature.

$$Z^* = Z' - jZ'' \tag{1}$$

$$M^* = M' + jM'' = j\omega C_0 Z^* = j\omega C_0 Z' - \omega C_0 Z''$$
 (2)

where Z' and Z'' are the real and imaginary parts of complex electric impedance Z^* , and M' and M'' are the real and imaginary parts of complex electrical modulus M^* , respectively. In these expressions, ω is the angular frequency $(2\pi f)$ of the applied ac phase, C_0 is the vacuum capacitance of the measuring cell, $C_0 = \varepsilon_0 A/l$, where ε_0 is the permittivity of free space $(8.854 \times 10^{-14} \, \text{F/cm})$, A and l are the cell area and thickness, respectively. The individual grain and grain boundary contributions can be exhibited by analyzing the impedance and electrical modulus of the cofired composite MLV. Figure 5a,b shows impedance spectroscopy measurements in the -75 to -25 and 25-75 °C temperature ranges, respectively.

It can be understood from the impedance measurements, there are clearly two contributions (grain and grain boundary) at low temperature, while after relatively higher than 50 °C temperature, the multilayer composite device has one contribution (grain). It is important to note that because of the presence of a polymer, the operating temperature of the device need to be carefully chosen to assure its reliability. Indeed, one should also consider thermal contributions induced by the electrical field. 32 By comparing the impedance data of the Cu-co-fired multilayer devices sintered at 220 °C (Figure S3a in the Supporting Information) and 120 °C, differences can be observed because of the grain boundary contribution of polymer in composites. The small resistant value of the MLV sintered at 220 °C corresponds to the semiconducting ZnO grains (Figure S3a in the Supporting Information). The magnitude of the resistance increases from M Ω -to G Ω -ranges when the sintering temperature decreases. The imaginary part of electrical modulus of the multilayer composite varistor, (M''), measured as a

function of the frequency at different temperatures (Figure 5c) also provides relevant information. The electrical modulus has two relaxation peaks between -75 and 25 °C and a shift of peaks to higher frequency. This is due to a thermally activated process where electrons and holes can be transported across the double Schottky barrier at the ZnO grain boundaries.³³ The activation energies, E_a , from these two peaks are 0.27 and 0.29 eV for high frequency and low frequency, respectively. The E_a of 0.29 eV is fairly reasonable for singly ionized oxygen vacancy in the ZnO grain. 34 Although there are few reported data for E_a of ZnO/PEI interface, 0.29 eV is relatively lower than the ZnO/ZnO interface (grain boundary) in the conventionally sintered ZnO.³⁵ The peak position of the modulus peak is defined as f_r = $\sigma/2\pi\varepsilon$, where σ and ε are conductivity and permittivity of constituent elements (e.g. grain, grain boundary), respectively. The difference in two peak positions is approximately ~ 3.5 orders of magnitude of difference in all the temperature range. Assuming ε of the grain and of grain boundary to be similar, this can be interpreted that the low-frequency peak that is associated with grain boundary impedance possesses 10³ to 10⁴ higher resistance than the other (grain).

Also, the MLV device sintered at 120 °C and the $G\Omega$ range resistances at a low frequency are associated with the presence of the PEI polymer at the interface between ZnO grains. It should be noted that no relaxation peaks were observed for the MLV device sintered at 220 °C (Figure S3b in the Supporting Information). It can be associated with conductive free carbon that might be present at the interface between grain boundaries following the thermal decomposition of the polymer (Figure 2), and this may have caused the multilayer device having an ohmic behavior (Figure S4 in the Supporting Information).

The characteristic I-V measurements can be used for qualifying the varistors, the nonlinear I-V characteristics occurred directly between the grain boundaries (polymers)

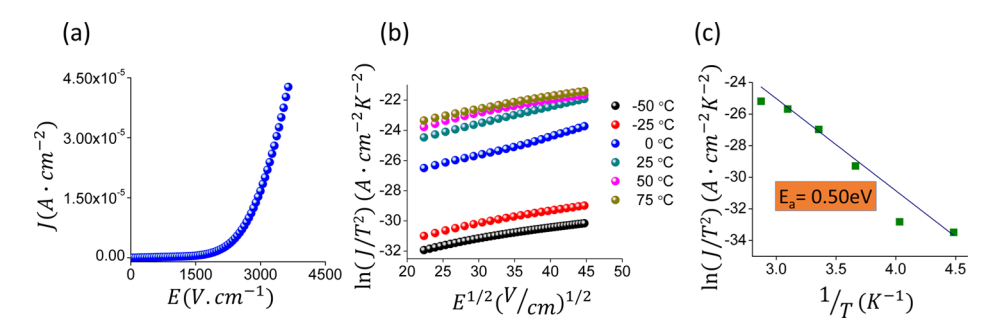


Figure 6. (a) J-E curve, (b) Schottky thermionic emission process as function of temperature, and (c) calculated activation energy.

and ZnO grains. The nonlinear relation between the voltage and current is generally given using eq 3

$$I = kV^{\alpha} \tag{3}$$

where I is the current, V is the voltage, k is a constant, and α is the nonlinear coefficient, and it represents the degree of nonlinearity that is one of the most valuable parameters for varistors. $\alpha = 1$ refers to an ohmic resistor behavior, and $\alpha > 1$ refers to a nonlinear I-V behavior which is typical for varistors. ³⁶ Figure 6a depicts the dc current density—electrical field (J-E) characteristic of the Cu-cofired multilayer nanocomposite varistor that is sintered at 120 °C for 30 min. The *J–E* curve shows an ohmic relation like the resistor behavior in the preswitch region at a low electrical field, and when it exceeds the critical voltage, the resistivity of the varistor increases and the I-E graph shows nonlinear properties. It is believed that nonlinear characteristics are triggered by the ZnO/PEI interface as evidenced by impedance spectroscopy (Figure 5). The calculated non-linear coefficient, α , of the ZnO/PEI composite multilayer is 5.30. This value is higher than $\alpha \approx 2$ in ZnO-Bi₂O₃-based varistors; ^{37,38} however, it is still limited when it compares with the commercial ZnO-MOs-based varistor. In follow up experiments, we will study the influence of the composite composition and the use of, for example, Bi₂O₃-, Mn₂O₃-, CoO-, Sb₂O₃-, or Al₂O₃- doped ZnO powders already deployed in conventional varistor systems to increase the nonlinear properties of devices.³³

The 5-10 nm thick polymer at the ZnO grain boundary (see in Figure 4d) creates a barrier and follows Schottky thermionic emission in terms of the non-ohmic behavior. Therefore, the J-E graph can be explained by Schottky thermionic emission, that is, the temperature-dependent region in terms of activation energy, so the activation energy is calculated from eq 4

$$J = AT^2 \exp(\beta E^{1/2} - q\phi) \tag{4}$$

where J is the current density, A is a constant, T is the absolute temperature, β is a constant, E is the electric field, q is the charge, and ϕ is the Schottky barrier height. Figure 6b shows the current density-electrical field graph of the MLV composite that is plotted according to eq 4 as a function of temperature from -50to 75 °C. The activation energy of the ZnO/PEI multilayer composite calculated from Figure 6c is 0.50 eV, which is in good agreement with activation energies of ZnO-metal oxides-based varistors.³⁹ The difference between this value and the earlier value obtained from modulus spectroscopy is thought to be due to a difference in measurement methods, as it is well known in research on semiconductors. 40 Another possible reason is that energy barrier attributed to 0.50 eV is not observed in Figure 5 because it was outside the measured temperature-frequency range. Unfortunately, the temperature range of Figure 5 was limited by the stability of PEI, and the frequency lower than 0.01

Hz was also unrealistic for the spectroscopic measurement. In any case, it remains true that the ZnO/PEI interface formed a potential barrier, providing enhanced resistance and nonlinear I-V characteristics. Thus, we avoid further discussion in this paper. Beyond all discussion, it is important to point out that Figures 4 and 6 reflect the main idea of this novelty, and it is an excellent facility to demonstrate the micro/nano structure–electrical property relationship by grain boundary engineering.

4. CONCLUSIONS

The fabrication of a functional MLV device at a record low temperature was demonstrated using the CSCC technology. In this MLV device, a small volume fraction of PEI polymer is used to engineer ZnO grain boundaries, and a base metal was used as internal electrodes. One of the key points in the process was the use of a polypropylene carbonate (QPAC-40) binder system to fabricate the ZnO/PEI tape. This binder system allowed a clean binder burnout procedure at low temperature under N₂-H₂ forming gas to avoid oxidation of the base metal electrode. The fabricated device highlighted a clean interface between the metal and ceramic/polymer composite, observed by STEM-EDS mapping. A nonlinear current-voltage response following the creation of the double Schottky barrier was demonstrated in the structure-property relationship investigation. The concept presented in this study offers the possibility to fabricate multilayer devices for other types of applications at low temperatures.

ASSOCIATED CONTENT

5 Supporting Information

The Supporting Information is available free of charge at https://pubs.acs.org/doi/10.1021/acsaelm.0c00225.

SEM—EDS micrograph of MLV sintered at 220 °C for 30 min; STEM—EDS figures from the vicinity of ceramic/polymer/metal and ceramic/polymer composite interface of multilayer sintered at 220 °C for 30 min; impedance and electrical modulus spectroscopy of Cu-co-fired ZnO/PEI; *J—E* curve of the Cu-co-fired ZnO/PEI multilayer composite device sintered at 220 °C for 30 min; schematic representation of the ZnO tape and printed Cu paste, multilayer, and electrode area, and layer thickness and electrode thickness of MLV devices after sintering at 120 °C (S5) (PDF)

AUTHOR INFORMATION

Corresponding Author

Sinan Dursun — Materials Research Institute and Department of Material Science and Engineering, The Pennsylvania State *University, University Park, Pennsylvania 16802, United States;* orcid.org/0000-0001-9270-3368; Email: sxd448@psu.edu

Authors

Kosuke Tsuji — Materials Research Institute and Department of Material Science and Engineering, The Pennsylvania State University, University Park, Pennsylvania 16802, United States

Sun Hwi Bang – Materials Research Institute and Department of Material Science and Engineering, The Pennsylvania State University, University Park, Pennsylvania 16802, United States

Arnaud Ndayishimiye — Materials Research Institute and Department of Material Science and Engineering, The Pennsylvania State University, University Park, Pennsylvania 16802, United States; orcid.org/0000-0003-3853-8239

Clive A. Randall – Materials Research Institute and Department of Material Science and Engineering, The Pennsylvania State University, University Park, Pennsylvania 16802, United States

Complete contact information is available at: https://pubs.acs.org/10.1021/acsaelm.0c00225

Notes

The authors declare no competing financial interest.

ACKNOWLEDGMENTS

This material is based on the work supported by the National Science Foundation, as part of the Center for Dielectrics and Piezoelectrics under grant nos. IIP-1361571 and 1361503, and IIP-1841453 and 1841466. We wish to thank Shoei Chemical Inc. for supplying copper powders, Empower Materials for supplying QPAC binder polymers, and SABIC for supplying the PEI polymer. Any opinions, findings, conclusions, or recommendations expressed in this material are those of the author(s) and do not necessarily reflect the views of the Foundation. The authors also would like to acknowledge Steve Perini, Jeff Long, Julie Anderson, Manuel Villalpando, and Ke Wang for their technical support during this study.

REFERENCES

- (1) Clarke, D. R. Varistor Ceramics. *J. Am. Ceram. Soc.* **1999**, 82, 485–502.
- (2) Toal, F. J.; Dougherty, J. P.; Randall, C. A. Processing and Electrical Characterization of a Varistor-Capacitor Cofired Multilayer Device. *J. Am. Ceram. Soc.* **2005**, *81*, 2371–2380.
- (3) Kuo, S.-T.; Tuan, W.-H. Grain Growth Behaviour of ZnO-Based Multilayer Varistors. *J. Eur. Ceram. Soc.* **2010**, *30*, 525–530.
- (4) Hong, K.; Lee, T. H.; Suh, J. M.; Yoon, S.-H.; Jang, H. W. Perspectives and Challenges in Multilayer Ceramic Capacitors for next Generation Electronics. J. Mater. Chem. C 2019, 7, 9782–9802.
- (5) Cologna, M.; Contino, A. R.; Sglavo, V. M.; Modena, S.; Ceschini, S.; Bertoldi, M. Curvature Evolution and Control in Anode Supported Solid Oxide Fuel Cells; John Wiley & Sons, Ltd, 2010; pp 95–104.
- (6) Green, D. J.; Guillon, O.; Rödel, J. Constrained Sintering: A Delicate Balance of Scales. *J. Eur. Ceram. Soc.* **2008**, 28, 1451–1466.
- (7) Chiang, M.-J.; Jean, J.-H.; Lin, S.-C. Effects of Green Density Difference on Camber Development during the Cofiring of a Bi-Layer Glass-Based Dielectric Laminate. *Mater. Chem. Phys.* **2011**, *128*, 413–417.
- (8) Hsu, R.-T.; Jean, J.-H. Key Factors Controlling Camber Behavior during the Cofiring of Bi-Layer Ceramic Dielectric Laminates. *J. Am. Ceram. Soc.* **2005**, *88*, 2429–2434.
- (9) Cai, P. Z.; Green, D. J.; Messing, G. L. Constrained Densification of Alumina/Zirconia Hybrid Laminates, I: Experimental Observations of Processing Defects. *J. Am. Ceram. Soc.* **2005**, *80*, 1929–1939.
- (10) Guo, J.; Guo, H.; Baker, A. L.; Lanagan, M. T.; Kupp, E. R.; Messing, G. L.; Randall, C. A. Cold Sintering: A Paradigm Shift for

- Processing and Integration of Ceramics. *Angew. Chem., Int. Ed.* **2016**, *55*, 11457–11461.
- (11) Bouville, F.; Studart, A. R. Geologically-Inspired Strong Bulk Ceramics Made with Water at Room Temperature. *Nat. Commun.* **2017**, *8*, 14655.
- (12) Funahashi, S.; Guo, J.; Guo, H.; Wang, K.; Baker, A. L.; Shiratsuyu, K.; Randall, C. A. Demonstration of the Cold Sintering Process Study for the Densification and Grain Growth of ZnO Ceramics. J. Am. Ceram. Soc. 2017, 100, 546–553.
- (13) Sengul, M. Y.; Guo, J.; Randall, C. A.; Van Duin, A. C. T. Water-Mediated Surface Diffusion Mechanism Enables the Cold Sintering Process: A Combined Computational and Experimental Study. *Angew. Chem., Int. Ed.* **2019**, *58*, 12420–12424.
- (14) Ndayishimiye, A.; Tsuji, K.; Wang, K.; Bang, S. H.; Randall, C. A. Sintering Mechanisms and Dielectric Properties of Cold Sintered (1-x) SiO2 x PTFE Composites. *J. Eur. Ceram. Soc.* **2019**, *39*, 4743–4751.
- (15) Gonzalez-Julian, J.; Neuhaus, K.; Bernemann, M.; Pereira da Silva, J.; Laptev, A.; Bram, M.; Guillon, O. Unveiling the Mechanisms of Cold Sintering of ZnO at 250 °C by Varying Applied Stress and Characterizing Grain Boundaries by Kelvin Probe Force Microscopy. *Acta Mater.* 2018, 144, 116–128.
- (16) Ashby, M. F. A First Report on Sintering Diagrams. *Acta Metall.* **1974**, 22, 275.
- (17) Guo, J.; Zhao, X.; Herisson De Beauvoir, T.; Seo, J.-H.; Berbano, S. S.; Baker, A. L.; Azina, C.; Randall, C. A. Recent Progress in Applications of the Cold Sintering Process for Ceramic—Polymer Composites. *Adv. Funct. Mater.* **2018**, 28, 1801724.
- (18) Ndayishimiye, A.; Grady, Z. A.; Tsuji, K.; Wang, K.; Bang, S. H.; Randall, C. A. Thermosetting Polymers in Cold Sintering: The Fabrication of ZnO Polydimethylsiloxane Composites. *J. Am. Ceram. Soc.* **2020**, *103*, 3039.
- (19) Guo, J.; Baker, A. L.; Guo, H.; Lanagan, M.; Randall, C. A. Cold Sintering Process: A New Era for Ceramic Packaging and Microwave Device Development. J. Am. Ceram. Soc. 2017, 100, 669–677.
- (20) Lee, W.; Lyon, C. K.; Seo, J. H.; Lopez-hallman, R.; Leng, Y.; Wang, C. Y.; Hickner, M. A.; Randall, C. A.; Gomez, E. D. Ceramic Salt Composite Electrolytes from Cold Sintering. *Adv. Funct. Mater.* **2019**, *29*, 1807872.
- (21) Funahashi, S.; Guo, H.; Guo, J.; Baker, A. L.; Wang, K.; Shiratsuyu, K.; Randall, C. A. Cold Sintering and Co-Firing of a Multilayer Device with Thermoelectric Materials. *J. Am. Ceram. Soc.* **2017**, *100*, 3488–3496.
- (22) Zhao, X.; Guo, J.; Wang, K.; Herisson De Beauvoir, T.; Li, B.; Randall, C. A. Introducing a ZnO–PTFE (Polymer) Nanocomposite Varistor via the Cold Sintering Process. *Adv. Eng. Mater.* **2018**, *20*, 1700902.
- (23) de Beauvoir, T. H.; Dursun, S.; Gao, L.; Randall, C. New Opportunities in Metallization Integration in Cofired Electroceramic Multilayers by the Cold Sintering Process. *ACS Appl. Electron. Mater.* **2019**, *1*, 1198–1207.
- (24) Bang, S. H.; Tsuji, K.; Ndayishimiye, A.; Dursun, S.; Seo, J. H.; Otieno, S.; Randall, C. A. Toward a Size Scale-up Cold Sintering Process at Reduced Uniaxial Pressure. *J. Am. Ceram. Soc.* **2020**, *103*, 2322.
- (25) Gao, L.; Ko, S.-W.; Guo, H.; Hennig, E.; Randall, C. A. Demonstration of Copper Co-Fired (Na, K)NbO₃ Multilayer Structures for Piezoelectric Applications. *J. Am. Ceram. Soc.* **2016**, 99, 2017–2023.
- (26) Chen, B.-K.; Su, C.-T.; Tseng, M.-C.; Tsay, S.-Y. Preparation of Polyetherimide Nanocomposites with Improved Thermal, Mechanical and Dielectric Properties. *Polym. Bull.* **2006**, *57*, 671–681.
- (27) Socrates, G. Infrared and Raman Characteristic Group Frequencies: Tables and Charts, 3rd ed.; Wiley, 2004; p 149.
- (28) Farong, H.; Xueqiu, W.; Shijin, L. The Thermal Stability of Polyetherimide. *Polym. Degrad. Stab.* 1987, 18, 247–259.
- (29) Barsoukov, E.; Macdonald, J. R. *Impedance Spectroscopy: Theory, Experiment, and Applications,* 2nd ed.; A John Wiley & Sons, Inc., Publication: Hoboken, New Jersey, 2005, p 205.

- (30) Sinclair, D. C.; West, A. R. Impedance and Modulus Spectroscopy of Semiconducting BaTiO3 Showing Positive Temperature Coefficient of Resistance. *J. Appl. Phys.* **1989**, *66*, 3850–3856.
- (31) Bayer, T. J. M.; Wang, J.-J.; Carter, J. J.; Moballegh, A.; Baker, J.; Irving, D. L.; Dickey, E. C.; Chen, L.-Q.; Randall, C. A. The Relation of Electrical Conductivity Profiles and Modulus Data Using the Example of STO:Fe Single Crystals: A Path to Improve the Model of Resistance Degradation. *Acta Mater.* **2016**, *117*, 252–261.
- (32) Gupta, T. K. Application of Zinc Oxide Varistors. *J. Am. Ceram.* Soc. 1990, 73, 1817–1840.
- (33) He, J. Metal Oxide Varistors: from Microstructure to Macro-Characteristics; Wiley-VCH Verlag GmbH & Co. KGaA: Weinheim, Germany, 2019.
- (34) Hong, Y. W.; Kim, J. H. Impedance and Admittance Spectroscopy of Mn₃O₄-Doped ZnO Incorporated with Sb₂O₃ and Bi₂O₃. Ceram. Int. **2004**, 30, 1307–1311.
- (35) West, A. R.; Andres-Verges, M. Impedance and Modulus Spectroscopy of ZnO Varistors. J. Electroceramics 1997, 1, 125–132.
- (36) Levinson, L. M.; Philipp, H. R. The Physics of Metal Oxide Varistors. J. Appl. Phys. 1975, 46, 1332–1341.
- (37) Zhao, X.; Li, J.; Li, H.; Li, S. Intrinsic and Extrinsic Defect Relaxation Behavior of ZnO Ceramics. *J. Appl. Phys.* **2012**, *111* (). https://doi.org/ DOI: 10.1063/1.4729804.
- (38) Zhang, Y.; Jung, J.-I.; Luo, J. Thermal Runaway, Flash Sintering and Asymmetrical Microstructural Development of ZnO and ZnO-Bi₂O₃ under Direct Currents. *Acta Mater.* **2015**, *94*, 87–100.
- (39) Zhao, X.; Liao, R.; Liang, N.; Yang, L.; Li, J.; Li, J. Role of Defects in Determining the Electrical Properties of ZnO Ceramics. *J. Appl. Phys.* **2014**, *116*, 014103.
- (40) Sze, S. M.; Ng, K. K. Physics and Properties of Semiconductors-A Review. In *Physics of Semiconductor Devices*; John Wiley & Sons, Inc.: Hoboken, NJ, USA, 2006; pp 5–75.